

# Confined Metastable 2-Line Ferrihydrite for Affordable Point-of-Use Arsenic-Free Drinking Water

Avula Anil Kumar, Anirban Som, Paolo Longo, Chennu Sudhakar, Radha Gobinda Bhuiin, Soujit Sen Gupta, Anshup, Mohan Udhaya Sankar, Amrita Chaudhary, Ramesh Kumar, and Thalappil Pradeep\*

Nanomaterials with intrinsically high surface energy, prepared using naturally abundant ingredients can be helpful in creating green products.<sup>[1]</sup> Several nanoscale materials have been prepared recently for applications of water purification, which exhibit improved performance vis-à-vis existing compositions, thereby enhancing the effectiveness of point-of-use water purifiers. However, such materials cannot be used in the native form for water purification because of difficulties in particle separation, potential danger in view of their leaching into the purified water,<sup>[2]</sup> and poor hydraulic conductivity of the filtration device. Examples such as activated alumina,<sup>[3]</sup> activated carbon,<sup>[4,5]</sup> iron oxide,<sup>[5,6]</sup> silicon dioxide,<sup>[7]</sup> granular ferric hydroxide (GFH),<sup>[8]</sup> reduced graphene oxide (RGO)-metal/metal oxide composites,<sup>[9–11]</sup> and magnetite-reduced graphene oxide composite (M-RGO)<sup>[12]</sup> are well known in the literature. Important requirement in the context of arsenic (As) removal media is the simultaneous removal of both As(III) and As(V) species present in natural water with enhanced kinetics, enabling fast delivery of clean water.

Hydrous nanoscale metal oxides are available abundantly in nature,<sup>[13]</sup> they are formed in geological time scale by slow crystallization, often assisted by mild temperature and pressure variations. However, this leads to the destruction of adsorption sites. Researchers have looked at new methods to synthesize iron oxide/hydroxide/oxyhydroxide compositions in the laboratory and used them for water purification.<sup>[13]</sup> They exist in rich variety of structures and hydration states. They are commonly fine-grained (nanophase) and poorly crystalline. The competition between surface energies and energetics of phase transformation suggests that metastable micrometer-sized or larger polymorphs can often be stabilized at the nanoscale. Such size-driven crossovers in stability help to explain patterns of occurrence of different iron oxides in nature.<sup>[14]</sup> Many of

them have been shown to be effective for the removal of As(III) and As(V) and such chemistry for arsenic remediation has been investigated.<sup>[15–17]</sup> Here, we present a simple method to maintain the metastable 2-line ferrihydrite phase at room temperature by confining it in biopolymeric cages. This material is termed as confined metastable 2-line ferrihydrite (CM2LF) having unprecedented adsorption capacity for both As(III) and As(V) in field conditions. We describe an affordable water purification device using such a composite, developed over several years, undergoing large scale field trials in India, as a potential solution for the eradication of arsenic from drinking water.<sup>[18]</sup> The material is green and causes no additional environmental impact for its production and in the course of use.

CM2LF appears to be largely amorphous in transmission electron microscopy (TEM) (Figure 1A). We believe that this is due to the small size of the crystalline domains of the material which might not be located under high resolution transmission electron microscopy (HRTEM). Nanoscale features are evident in the image, which are uniform throughout. Fast Fourier transform (FFT) diffraction pattern is shown in inset a<sub>1</sub>. The phase continues to remain the same at ambient conditions, but gradually gets converted to more stable forms of hematite ( $\alpha$ -Fe<sub>2</sub>O<sub>3</sub>, rhombohedral, JCPDS 89-8103) and goethite ( $\alpha$ -FeOOH, orthorhombic, JCPDS 81-0464)<sup>[19]</sup> upon electron beam irradiation. FFT diffraction pattern (Figure 1Bb<sub>1</sub>) of the irradiated material along with lattice resolved images of these phases (inset b<sub>2</sub>, b<sub>3</sub>, and b<sub>4</sub>) are shown in Figure 1B. The phases were confirmed by the lattice planes of hematite (b<sub>2</sub>, b<sub>4</sub>) and goethite (b<sub>3</sub>), which matches with the Cambridge crystallographic data (CCD). Electron beam induced time dependent HRTEM images of initial CM2LF, As(III) adsorbed and As(V) adsorbed samples show the conversion of amorphous to crystalline state. Lattice resolved images of these samples are shown in Figure S1 of the Supporting Information. Scanning electron microscope (SEM) image of the initial granular material is shown in Figure S2A (Supporting Information). The material was kept in water and was found to be stable even after six months without any leaching of Fe. Stability of the composition is attributed to abundant –O and –OH functional groups of chitosan, which help in the formation of metastable amorphous metal oxyhydroxide and also ensure strong covalent binding of the nanoparticle surface to the matrix. Iron oxyhydroxide nanoparticles bind to chitosan network, possibly through covalent sharing of oxygen, leading to metastable 2-line ferrihydrite phase similar to the formation of ALOOH nanoparticles in chitosan network, comparable to the mechanism reported by Sankar et al.<sup>[20]</sup> Figure 1C<sub>1</sub> shows the annular dark-field

A. A. Kumar, A. Som, C. Sudhakar, Dr. R. G. Bhuiin, S. Sen Gupta, Anshup, M. U. Sankar, A. Chaudhary, R. Kumar, Prof. T. Pradeep  
DST Unit of Nanoscience (DST UNS)  
and Thematic Unit of Excellence (TUE)  
Department of Chemistry  
Indian Institute of Technology Madras  
Chennai 600036, India  
E-mail: pradeep@iitm.ac.in

Dr. P. Longo  
Gatan Inc.  
5794 W Las Positas Blvd, Pleasanton, CA 94588, USA



DOI: 10.1002/adma.201604260

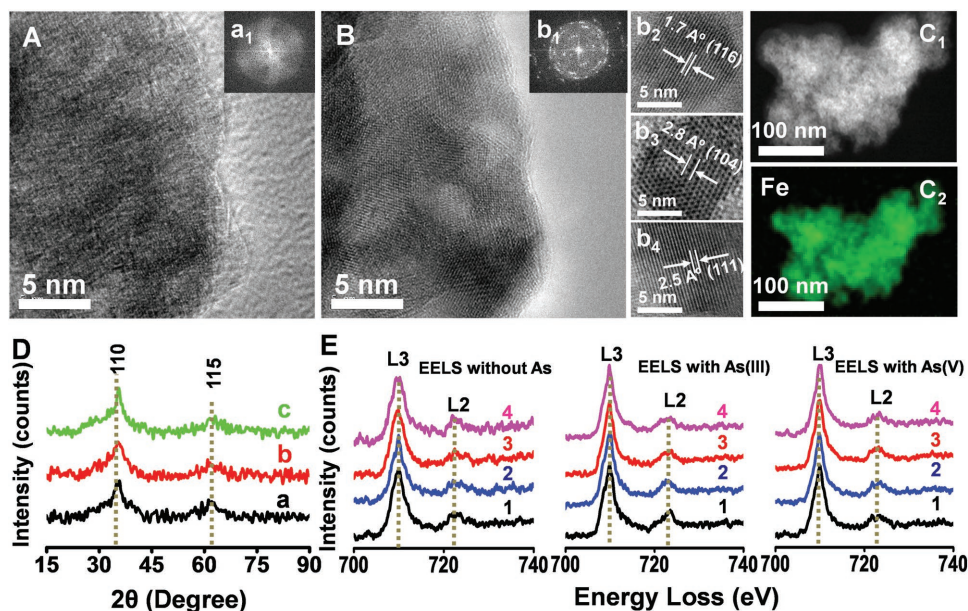


**Figure 1.** A) HRTEM amorphous feature of CM2LF along with dark field image (inset  $a_1$ ). B) Beam induced crystallization of CM2LF along with dark field image and lattice resolved images (inset  $b_1$ ,  $b_2$ ,  $b_3$ , and  $b_4$ ).  $C_1$  and  $C_2$ ) ADF-STEM image and Fe elemental mapping images of the initial material. D) XRD of CM2LF (a) before As adsorption (initial material), (b) after As(III), and (c) after As(V) adsorption. E) Dual EELS spectrum of iron L3, L2 region (Fe L3, L2) of CM2LF in four different locations (1, 2, 3, and 4) of the same sample.

scanning transmission electron microscopy (ADF-STEM) image of the initial composite (i.e., before arsenic adsorption) and elemental map (Figure 1C<sub>2</sub>) of the image shows that Fe is uniformly distributed in the material. The ADF-STEM images along with the elemental maps of O, Fe, and As after the adsorption of As(III) and As(V) onto the composite are shown in Figure S2B and S2C (Supporting Information), respectively. Uniform distribution of As is seen in the material. Powder X-ray diffractogram (PXRD) pattern of the adsorbent shows the 2-line ferrihydrite phase (Figure 1D), which matches with the CCD (JCPDS, 46-1315). As(III) and As(V) adsorption does not change the PXRD profiles. No new phase was observed in PXRD of the used materials (Figure 1Db,c) which clearly shows the long-term stability of CM2LF nanocomposite in water.

Infrared spectroscopic investigation of CM2LF shows that the distinct chitosan features at  $1662\text{ cm}^{-1}$  due to C=O of amide I,  $1329\text{ cm}^{-1}$  due to N–H deformation and C–N stretching vibration and  $1157\text{ cm}^{-1}$  corresponding to asymmetric C–O–C stretching<sup>[21,22]</sup> are shifted to 1636, 1375, and  $1069\text{ cm}^{-1}$ , respectively indicating strong interaction with the ferrihydrite particles (Figure S3, Supporting Information). NaHAsO<sub>2</sub> shows As–O stretching peaks at 843 and  $1210\text{ cm}^{-1}$  which are blueshifted to 808 and  $1070\text{ cm}^{-1}$  after adsorption. Similarly, Na<sub>2</sub>HAsO<sub>4</sub> shows peaks at 851 and  $1175\text{ cm}^{-1}$  due to As–O stretching, which are blueshifted to 808 and  $1070\text{ cm}^{-1}$  after interaction with CM2LF. These are shown in Figure S3 (Supporting Information).

Dual electron energy loss spectroscopy (Dual EELS) studies were performed to understand local effects in view of nanoscale nature of the materials (Figure 1E). However, no drastic changes were observed in the L2, L3 regions of Fe 2p edges upon As(III)/As(V) interaction, which may be correlated with the X-ray photoelectron spectroscopy (XPS). Fe 2p does not

undergo a significant chemical shift upon As(III)/As(V) interaction (to be discussed later in the text). We believe that this is due to adsorption, which leads to no significant chemical changes.

CM2LF is stable in dry and wet conditions. Figure S4 (Supporting Information) shows the Young's moduli of the materials evaluated to be 2.42 and 2.64 MPa in dry and wet conditions, respectively and the values are comparable to standard Ennore sand used as reference.<sup>[23]</sup> The corresponding data of Mohr–Coulomb failure pattern are shown in Figure S5 (Supporting Information). The data show that CM2LF has higher shear strength in comparison to sand (friction angle,  $\phi = 34.68^\circ$ ). This stability, in loose and wet conditions, is important in device fabrication. Indirectly, this also suggests that the material does not leach out anything which is desirable for a material used for drinking water purification.

CM2LF due to its inherently porous structure and high surface area ( $172\text{ m}^2\text{ g}^{-1}$ ) can be used to make a point-of-use arsenic water purifier. Its structure, while allowing ion penetration within, protects the composite as a whole from scale forming species, so as to maintain uptake kinetics. The synthesized material exhibits inherent green strength and has an uptake capacity of  $100\text{ mg g}^{-1}$  in the field conditions, the highest arsenic adsorption capacity known so far, allowing the creation of affordable water purifiers. While FeOOH in its various forms are known to uptake arsenic in both As(III) and As(V) forms, a point of use gravity fed purifier requires highest uptake capacity to be viable. Uptake capacity of CM2LF for As(III) and As(V) follows Langmuir adsorption isotherm; the data are presented in Figure S6 (Supporting Information).

After evaluating the performance of the material in batch experiments, a prototype filter was developed. About 60 g of the composite (particle size  $\approx 72\text{ }\mu\text{m}$ ) was packed in a water

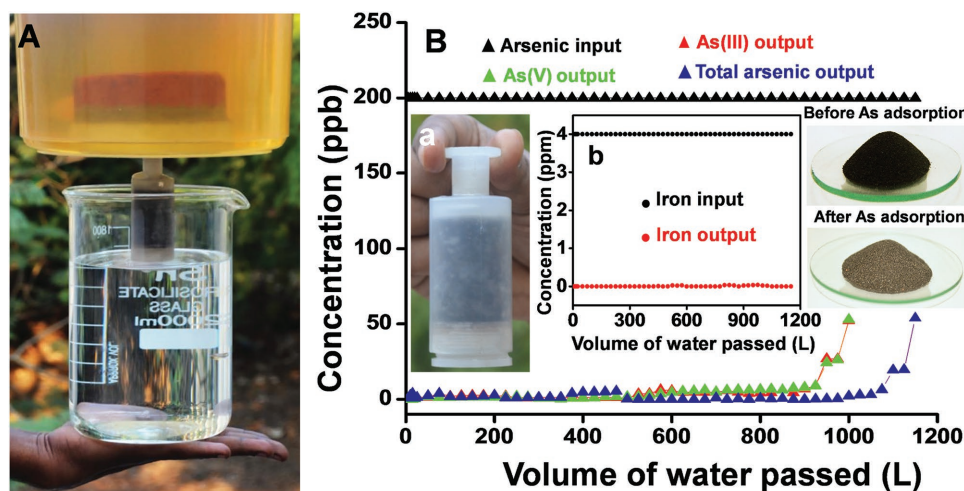


**Figure 2.** Set-up used for filtration containing arsenic (As(III + V)) and iron (Fe(II + III)) contaminated water using a cartridge with the reported material, along with a porous clay prefilter. B) Arsenic concentration in the water using a 60 g cartridge with the input as shown in A), inset (a) is the cartridge having 20 g adsorbent, inset (b) is iron output for the same input. The photographs of granular CM2LF before (black) and after (brown) As adsorption are in the inset.

purification cartridge (diameter, 10 mm; height, 35 mm) and a filter was assembled in an antigravity fashion. Output water was analyzed after acidification (5%  $\text{HNO}_3$ ) and digestion, to ensure that all particulate matter that leached out, if at all, was also evaluated. In **Figure 2A**, we show a prototype used to conduct the experiments with over 1000 L of water at a flow rate of 12 to 15  $\text{mL min}^{-1}$ , under gravity. Slight variation in the flow rate in the course of the long experiment was due to difference in the pressure head of the input water container. A particulate filter made from porous clay was sandwiched with a nanocomposite filter, shown in **Figure 2Ba**. The input water contains 4  $\text{mg L}^{-1}$  (4 ppm) of Fe along with 200  $\mu\text{g L}^{-1}$  (200 ppb) of a mixture of As(III) and As(V) in 1:1 ratio. This 1:1 composition is as seen in nature<sup>[24]</sup> and referred to as As(mix). Various combinations of ions Fe(II), Fe(III), As(III), As(V), and As(mix) have been tried to understand the performance of the material.

The flow rates were optimized for best performance. Data in **Figure 2B** show that As(III), As(V), and As(mix) were removed below the World Health Organization (WHO) limit of 10  $\mu\text{g L}^{-1}$  for 1100 L synthetic and natural tap water samples using 60 g of the composite. The breakthrough was achieved at 1150 L, suggesting a capacity of 100  $\text{mg g}^{-1}$  for the material. This capacity is 1.4 to 7.6 times larger than the best values reported in the literature.<sup>[25]</sup> The composite after arsenic adsorption shows a mild change in color (**Figure 2B** inset). The TEM-energy dispersive spectroscopy (EDS) and SEM-EDS elemental mappings of As(III) and As(V) saturated composites are presented in **Figures S7** and **S8** (Supporting Information), respectively, which confirm the presence of adsorbed arsenic homogeneously. As arsenic is generally found with Fe in the natural environment, tests were conducted with an input load of 4  $\text{mg L}^{-1}$  Fe(II), which was removed to below the WHO limit of 300  $\mu\text{g L}^{-1}$  over the entire range of volume investigated (**Figure 2b**). Fe(II) was chosen as the input as natural ground water from a depth of 50–120 ft from where it was extracted typically in affected areas through tube wells, where Fe is present in the +2 form, due to anaerobic conditions. Fe(II) becomes

Fe(III) by aerial oxidation, intensifying the color of the water. Similar experiments were also conducted for Fe(III), As(III), As(V), and As(mix) separately and in various combinations of these and all the output values were below permissible limits. Experiments were conducted in the arsenic affected regions of West Bengal, Uttar Pradesh, Bihar, Assam, Jharkhand, Chhattisgarh, and Karnataka states of India in larger scale field trials as well, with similar results. Highest As contamination was seen in water sources of West Bengal, in the range of 200  $\mu\text{g L}^{-1}$ , although even higher concentrations are seen occasionally. Therefore, this was chosen as the input concentration in test conditions.

Experiments were conducted to remove arsenic using the porous clay composite alone in presence and absence of iron (Fe(II/III)). A decrease of 40  $\mu\text{g L}^{-1}$  was seen out of 200  $\mu\text{g L}^{-1}$  As (mix) input using the porous filter alone without Fe(II/III). It was never possible to meet the water quality norm of 10  $\mu\text{g L}^{-1}$  through this device in the absence of Fe(II)/Fe(III) both. Studies revealed that As(III)/As(V)/As(mix) removal was due to particulates of Fe(II)/Fe(III) hydroxides which could not be passed through the porous clay. Dynamic light scattering (DLS) studies showed the existence of three major particle size distributions in this water samples (**Figure S9**, Supporting Information). All the arsenic and iron containing water samples used for testing in this study were maintained at  $\text{pH} \approx 7.83$ .

Superior arsenic uptake capacity of the composite is due to its inherent structure. Arsenic uptake is uniform across the material and this does not change the inherent structure of the composite. This largely amorphous nature of the composite was also shown in the X-ray diffraction patterns (XRD), which reveals a metastable 2-line ferrihydrite structure in its most disordered form and it does not change upon As(III)/As(V) uptake. Uptake of arsenic appears to be surface adsorption as revealed by XPS studies (survey spectrum is shown in **Figure S10A** (Supporting Information), before and after As(III) and As(V) adsorption). Two broad peaks of Fe 2p were observed at 708.9 eV binding energy (BE) for Fe 2p<sub>3/2</sub> and 722.3 eV for

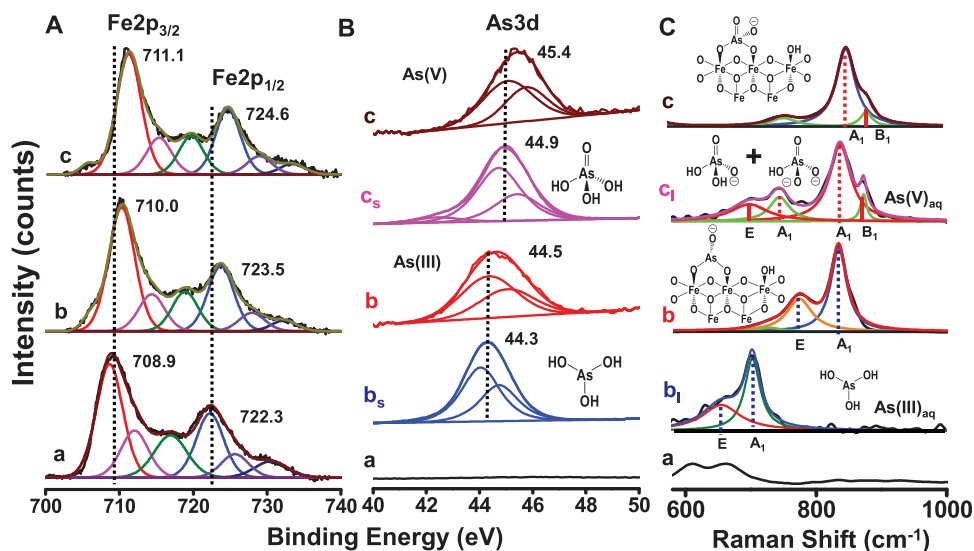


**Figure 3.** XPS of CM2LF showing A) Fe 2p and B) As 3d regions (a) before As adsorption, (b) after As(III) adsorption, and (c) after As(V) adsorption, independently compared with (b<sub>s</sub>) standard As(III) of solid NaAsO<sub>2</sub> and (c<sub>s</sub>) standard As(V) of solid Na<sub>2</sub>HAsO<sub>4</sub>·7H<sub>2</sub>O respectively. The lines in A and B indicate relative peak shifts. C) Raman spectrum of (a) CM2LF solid, (b<sub>1</sub> and c<sub>1</sub>) standard aqueous 100 × 10<sup>-3</sup> M solutions of As(III) and As(V) and (b and c) after adsorption of As(III) and As(V) on CM2LF. The structures in inset b<sub>1</sub> and c<sub>1</sub> show the speciation of As in solution at pH 7 and the structures in b and c show the probable structure of As(III/V) on CM2LF, respectively.

Fe 2p<sub>1/2</sub>, respectively for the initial material. The presence of satellite peak at 716.8 eV confirms +3 oxidation state of Fe (Figure 3Aa). The interaction of As(III)/As(V) does not change the oxidation state of Fe in CM2LF significantly. Similar Fe 2p doublet was observed at 710.0/723.5 and 711.1/724.6 eV, respectively for these samples, as shown in Figure 3Ab,c. Small change in the binding energy is due to the strong surface interaction of As with Fe(III). This explanation is supported by literature.<sup>[26,27]</sup> The C 1s core-level does not show any significant change while the other core levels, namely, As 3d (Figure 3B and Figure S10B, Supporting Information) and O 1s (Figure S10C, Supporting Information) show small changes upon arsenic interaction with CM2LF. There is a small shift of 0.2 and 0.5 eV, respectively for As(III) and As(V) to higher BE upon interaction with CM2LF, in comparison to the respective arsenic standards (Figure 3Bb<sub>s</sub>,c<sub>s</sub>). Data support physical interaction of As–O bonds with Fe in CM2LF. There is also a small shift in O 1s to higher BE upon As(III) and As(V) interaction with CM2LF (529.2 and 529.3 eV, respectively), in comparison to initial material (529.0 eV before arsenic adsorption), supporting strong interaction of O<sup>2-</sup> with Fe(III) and As(III)/As(V) upon adsorption (Figure S10C, Supporting Information).

Raman spectrum of CM2LF is shown in Figure S11a (Supporting Information). The peaks around 230 and 300 cm<sup>-1</sup> correspond to Fe–O and Fe–OH symmetric stretching. The standard arsenic materials, NaAsO<sub>2</sub> and Na<sub>2</sub>HAsO<sub>4</sub>·7H<sub>2</sub>O in solid state have characteristic peaks in the 700–900 cm<sup>-1</sup> window due to symmetric stretching (A<sub>1</sub>) of As–O bonds (see Figure S11, Supporting Information). As(III) in solution phase shows two peaks at pH 7 corresponding to the symmetric stretching mode A<sub>1</sub> at 702 cm<sup>-1</sup> and the antisymmetric stretching mode E at 650 cm<sup>-1</sup> due to the species, H<sub>3</sub>AsO<sub>3</sub> (C<sub>3v</sub> symmetry, Figure 3Cb<sub>1</sub>). A redshift in the peak position was observed for As(III) after interaction with CM2LF, the

peaks at 863 cm<sup>-1</sup> (A<sub>1</sub>) and 796 cm<sup>-1</sup> (E) are due to the strong bidentate binding interaction of As–O with Fe–O as shown in Figure 3Cb. Similarly, in solution phase at pH 7, As(V) has two species H<sub>2</sub>AsO<sub>4</sub><sup>-</sup> and HAsO<sub>4</sub><sup>2-</sup> in 1:1 ratio (ABCD<sub>2</sub> and AB<sub>2</sub>CD type molecules both having C<sub>s</sub> symmetry) exhibiting symmetric stretching (A<sub>1</sub>) at 836 and 743 cm<sup>-1</sup>, and symmetric bending (B<sub>1</sub> and E) at 875 and 696 cm<sup>-1</sup>; assigned respectively to these two species (Figure 3Cc<sub>1</sub>). Shifted peaks were observed at 852 cm<sup>-1</sup> (A<sub>1</sub>) and 884 cm<sup>-1</sup> (B<sub>1</sub>) after the interaction of As(V) with CM2LF. The near complete disappearance of the peaks at 680–750 cm<sup>-1</sup> confirms that H<sub>2</sub>AsO<sub>4</sub><sup>-</sup> converts to HAsO<sub>4</sub><sup>2-</sup> upon adsorption (Figure 3Cc). The interaction of HAsO<sub>4</sub><sup>2-</sup> with CM2LF is preferably bidentate in nature as shown in the inset of Figure 3Cc.

Figure 4 shows the mechanism of formation of CM2LF, where the ferric ions deposited on chitosan are converted to FeOOH nanoparticles (FeOOH NPs) upon incubation in alkaline medium at room temperature. It gradually makes nanocrystallites, confined in the chitosan network. The mechanical strength originates due to the formation of 3D cage-like structure of chitosan with embedded FeOOH NPs. These FeOOH NPs are accessible for water and dissolved ions. The interaction mechanism of As(III) and As(V) individually with CM2LF is shown Figures S12 and S13 (Supporting Information).

The effects of pH and common ion effect for the adsorption of As(III) and As(V) on CM2LF were studied. It was seen that pH in the range of 4–10 does not alter the adsorption capacity of CM2LF for As(III) and As(V), as shown in Figure S14 (Supporting Information). The effect of common ions on the As uptake is summarized in Table S1 (Supporting Information). CM2LF removes As(III) and As(V) efficiently even in the presence of other ions of relevance to drinking water. Total organic carbon (ToC) release from the components used in making

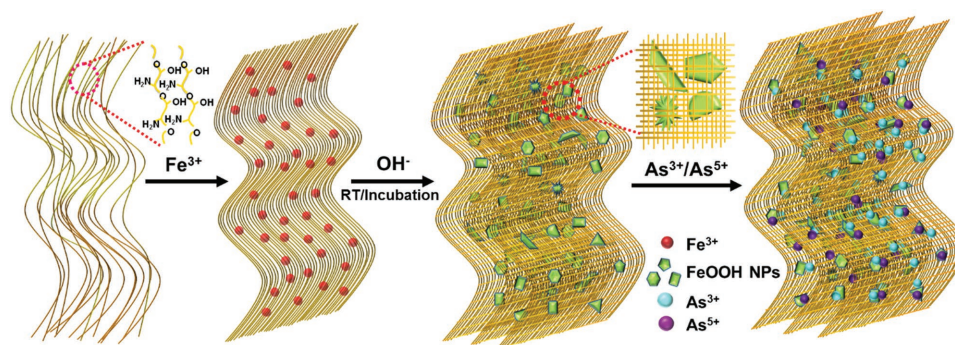


**Figure 4.** Schematic representation for the preparation of CM2LF and removal of As(III) and As(V) species from water.

CM2LF and the composite before and after As uptake was tested and these values were less than  $1 \text{ mg L}^{-1}$ , except for chitosan, as shown in Table S2 (Supporting Information). For chitosan, the ToC was  $3.39 \text{ mg L}^{-1}$  which may be due to the varying degree of polymerization; the smaller particles contribute to higher ToC. However, the acceptable United States Environmental Protection Agency (USEPA) limit for ToC in drinking water is  $4 \text{ mg L}^{-1}$ . Milli-Q water was used for experiments with CM2LF as the tap water routinely shows a ToC of  $8.60 \text{ mg L}^{-1}$ .

We have developed a reactivation protocol to regenerate the As saturated CM2LF. The composite was first soaked with  $\text{Na}_2\text{SO}_4$  solution and incubated for 1 h at room temperature. The pH of the solution was subsequently adjusted to 4 using 1 M HCl solution. The solution was further incubated for about 3–4 h. The material was then washed with DI water to remove excess  $\text{SO}_4^{2-}/\text{Cl}^-$  ions. This reactivated material was used for arsenic adsorption for the next cycle. Using the above mentioned protocol we have reactivated and reused the same material for next seven cycles without any loss of arsenic adsorption capacity. The data are shown in Figure S14C and S14D (Supporting Information) for As(III) and As(V), respectively. The toxicity characteristic leaching protocol (TCLP, <https://www.epa.gov/sites/production/files/2015-12/documents/1311.pdf>) studies were conducted using the saturated composites to know the leaching of adsorbed arsenic and iron. The tests showed a leaching of  $1 \mu\text{g L}^{-1}$  (total As),  $2 \mu\text{g L}^{-1}$  (total As) and  $24 \mu\text{g L}^{-1}$  (total Fe) for As(III), As(V) and iron, respectively.

The adsorption capacity of CM2LF was compared with pure ferrihydrite and chitosan separately with respect to the adsorbent dosage as shown in Figure S15 (Supporting Information). The maximum adsorption capacity of As was found to be  $36.9 \text{ mg g}^{-1}$  for ferrihydrite and  $8.0 \text{ mg g}^{-1}$  for chitosan in comparison to  $100.0 \text{ mg g}^{-1}$  for the composite. Performance data of CM2LF in batch experiments were also compared to other commercially available materials, viz., activated alumina, activated carbon, iron oxide ( $\text{Fe}_2\text{O}_3$ ), silicon dioxide ( $\text{SiO}_2$ ), GFH, and organic templated boehmite nanostructure (OTBN) are shown in Figures S16, S17, and S18 (Supporting Information). The arsenic adsorption capacities of commercial/noncommercial materials are reported as 15.9, 17.9, 20.2, 16.1, 70.0, and  $13.1 \text{ mg g}^{-1}$  for activated alumina,<sup>[3]</sup> activated carbon,<sup>[4,5]</sup> iron oxide,<sup>[5,6]</sup> silicon dioxide,<sup>[7]</sup> GFH,<sup>[8]</sup> and magnetite-reduced graphene oxide composite (M-RGO),<sup>[12]</sup> respectively. Data confirm that the arsenic removal capacity of CM2LF is 1.4 to 7.6 times better than

all the compared materials. XPS data of all these commercial/noncommercial materials upon As(III) and As(V) adsorption and comparison of the data with As(III) and As(V) standards are presented in Figures S19, S20, and S21 (Supporting Information). The As 3d peaks of some of the materials shift slightly to lower BE, while some others shift slightly to higher BE but none of them show a drastic shift in these peaks, similar to CM2LF.

A domestic water filtration unit was prepared as shown in the photograph in the inset of Figure S22a (Supporting Information). A filter used three stage water filtration – first, a  $0.5 \mu\text{m}$  polypropylene yarn wound cartridge filter for removal of particulates; second, iron removal media; and third, 900 g arsenic adsorbent, CM2LF. The water input and output are marked in the photograph. Performance data for the removal of arsenic and iron using three stage filtration, with a 1:1 ratio of As(III) and As(V), together at  $200 \mu\text{g L}^{-1}$  and either of Fe(II) and Fe(III) at  $4 \text{ mg L}^{-1}$ , as contaminants are shown in Figure S22A (Supporting Information), for a total volume of 6000 L water passed ( $>15 \text{ L per day}$  for a year). The output was below the WHO limit of 10 and  $300 \mu\text{g L}^{-1}$  for As and Fe, respectively, throughout the experiment. The inset, Figure S22b (Supporting Information) shows water flow rate from the unit at an applied pressure of 7 psi. Reduced quantity of adsorbent and higher flow rates are possible in the optimized design, at different levels of operation, especially in the community scale.

To summarize, As(III) and As(V) as well as mixed forms of the same could be effectively scavenged by a composite with fast kinetics allowing the creation of an affordable arsenic-free drinking water solution for point-of-use applications. The unprecedented large capacity in field conditions is attributed to the inherent structure of the composite with confined metastable 2-line ferrihydrite in biopolymer cages, which allows the creation of effective adsorption sites. The arsenic adsorption capacity of the composite is 1.4 to 7.6 times better than the available compositions. Synthesis of the composition involves simple raw materials and the process requires no electrical power and no organic solvents. With this material, arsenic-free drinking water can be delivered for a family of five at an estimated cost of US \$2 per year in resource limited settings.

## Experimental Section

**Materials:** Ferric chloride ( $\text{FeCl}_3 \cdot 6\text{H}_2\text{O}$ ), sodium hydroxide (NaOH), sodium sulphate ( $\text{Na}_2\text{SO}_4$ ), ferrous sulphate ( $\text{FeSO}_4 \cdot 7\text{H}_2\text{O}$ ), and ferric

sulphate ( $\text{Fe}_2(\text{SO}_4)_3 \cdot x\text{H}_2\text{O}$ ) were purchased from Rankem Glasswares and Chemicals, Pvt. Ltd. India. Biopolymer (Chitosan) was purchased from Pelican Biotech & Chemicals Labs Pvt. Ltd. India. Sodium arsenite ( $\text{NaAsO}_2$ ) and sodium arsenate ( $\text{Na}_2\text{HAsO}_4 \cdot 7\text{H}_2\text{O}$ ) were purchased from SD Fine Chemicals Limited. All chemicals were of analytical grade and were used without further purification. The porous filters developed by CSIR-Institute of Minerals and Materials Technology (IMMT) were purchased from Watson Envirotech Private Limited. Deionized water was used throughout the experiments unless otherwise mentioned.

**Synthesis of CM2LF:** The granular composites, composed of iron oxyhydroxide–chitosan nanostructures, were synthesized by a green synthetic route, which in general involves the hydrolysis of a metal precursor–chitosan complex using an alkaline medium followed by washing and drying at ambient conditions. Metal ion precursor used for the preparation of the composite was  $\text{Fe}^{3+}$ . All syntheses were carried out in deionized water, while natural ground water or tap water was used for testing.

An iron oxyhydroxide–chitosan nanostructure was synthesized as follows: About 0.13 g chitosan was dissolved in 10 mL, 1% HCl by continuous stirring for 12 h. This was precipitated at pH 9 using 0.2 M NaOH. About 0.5 g  $\text{Na}_2\text{SO}_4$  was added in one step. After 5 min of incubation, 10 mL, 1 M ferric hexachloride was added. The mixture was brought to pH 8, using 2 M sodium hydroxide by slow addition. The final composition was further incubated for about 12 h, at ambient temperature to embed the synthesized  $\text{FeOOH}$  nanoparticles in biopolymer cages. The resulting gel was washed with copious amount of water to remove soluble salts and was dried at room temperature (28–30 °C). The resulting composite, namely, CM2LF, was insoluble in water and appeared as black-red to brownish granules. The dried composite was crushed to specific sizes (optimized  $52 \times 72 \mu\text{m}$ ) and used for arsenic adsorption. The yield was 1.0 g. The method of preparation of the composite is water positive by two to three orders of magnitude; i.e., it produces 500 L of clean water for every 1 L of water consumed for its production. The as-prepared granular composite was stable and did not disintegrate in water for over two years.

The CM2LF prepared within the chitosan matrix, which induces structural integrity, is biodegradable and inexpensive. Other polymers such as banana silk can also be used for this purpose. The organic polymer acts as a template, controls the size of the particles, and gives mechanical strength to the composite after drying at room temperature. When the ferrihydrite nanoparticles were prepared within the matrix, they bind strongly with it, due to which no nanoparticles get into the purified water. It is well-known that hydrous iron oxide, as found in nature, exhibits reasonable mechanical strength (as they occur in crystalline form). In the case of CM2LF composite, it is largely amorphous. Here, the role of chitosan is crucial in improving the mechanical strength of CM2LF composite by binding with ferric oxyhydroxide nanocrystals. As 2-line ferrihydrite has been examined extensively in terms of its structure,<sup>[28,29]</sup> we focused only on its arsenic uptake properties.

**Testing Protocol for Arsenic Efficacy in Batch:** 25 mg of CM2LF was shaken with 100 mL of natural tap water (see Table S1 in the Supporting Information for water quality parameters). Arsenic removal efficiency of CM2LF was measured by spiking the natural tap water with As(III) and As(V) separately at a concentration of  $1.1 \text{ mg L}^{-1}$ . Thereafter, the water was left standing for 1.5 h and subsequently the leftover arsenic concentration in treated water was analyzed using inductively coupled plasma mass spectrometry (ICP-MS) after acidification with 5%  $\text{HNO}_3$ . Experiments with water filtration cartridges are described in the main text.

**Instrumentation:** HRTEM images of the sample were obtained with JEM 3010 (JEOL, Japan) operating at 200 kV with an ultrahigh resolution polepiece. Elemental mapping using TEM was done on an Oxford Semistem EDS system. The samples for HRTEM were prepared by dropping the dispersion on amorphous carbon films supported on a copper grid and subsequent drying. ADF-STEM measurements were carried out using a Gatan GIF Quantum ER fully loaded Tecnai F20. This analysis was carried out at 200 kV and the data were acquired in digital micrograph and the chemical analysis was carried out with 1 eV

energy resolution. This entire ADF-STEM analysis was carried out in Dual EELS mode to measure the accurate chemical shift. Identification of the phase(s) of all the samples was carried out by XRD (Bruker AXS, D8 Discover, USA) using  $\text{Cu K}\alpha$  radiation at  $\lambda = 1.5418 \text{ \AA}$ . XPS measurements were done using ESCA Probe TPD spectrometer of Omicron Nanotechnology. Polychromatic  $\text{Mg K}\alpha$  was used as the X-ray source ( $h\nu = 1253.6 \text{ eV}$ ). Samples were spotted as dropcast films on a sample stub. Constant analyzer energy of 20 eV was used for the measurements. Binding energy was calibrated with respect to C 1s at 284.5 eV. Surface enhanced Raman spectroscopy was performed using a CRM 200 micro Raman spectrometer of WiTec GmbH (Germany). The substrate was mounted on a sample stage of a confocal Raman spectrometer. The spectra were collected at 532 nm laser excitation. For Raman measurements, the corresponding nanomaterial/standard material (as in dried powder form)-coated glass substrates were analyzed keeping the laser and other parameters same. A super-notch filter placed in the path of the signal effectively cuts off the excitation radiation. The signal was then dispersed using a 600/1800 grooves per mm grating and the dispersed light was collected by a Peltier-cooled charge coupled device. Surface morphology, elemental analysis, and elemental mapping studies were carried out using a SEM equipped with EDS (FEI Quanta 200). For the SEM and EDS measurements, samples were spotted on an aluminum sample stub. Total arsenic and iron concentrations in water were detected using ICP-MS (Agilent Technologies, 7700x ICP-MS and PerkinElmer NexION 300X ICP-MS) with appropriate standards. Brunauer-Emmett-Teller (BET) surface area was measured using Micromeritics ASAP 2020. Samples were degassed at 200 °C for 4 h under vacuum and analysed at 77 K with ultra high pure nitrogen gas.

## Supporting Information

Supporting Information is available from the Wiley Online Library or from the author.

## Acknowledgements

The authors thank Avijit Baidya, Mohd. Azhardin Ganayee, Rahul Narayanan, and P. Srikrishnarka for taking photographs of the set-up used for arsenic testing, for their technical support in conducting Raman analysis, IR measurements, and help in making the Schematic and TOC figures, respectively. The authors thank Edamana Prasad and Madhu Babu for their help in measuring DLS measurements. The authors thank Ligy Philip and Ramprasad for help in ToC measurements. The authors also thank R. G. Robinson, Lini K. Nair, and Manu Santhanam (Department of Civil Engineering) for their help in conducting direct shear stress and compressive strength analyses. Radha Gobinda Bhuiin is currently working at University Erlangen-Nürnberg, Egerlandstr, Germany. National Centre for Catalysis Research at IIT Madras thanked for the BET analyses. Authors thank the Department of Science and Technology (Government of India) for constantly supporting our research program on nanomaterials.

Received: August 9, 2016

Revised: October 16, 2016

Published online: December 5, 2016

[1] T. Pradeep, Anshup, *Thin Solid Films* **2009**, 517, 6441.

[2] R. Damoiseaux, S. George, M. Li, S. Pokhrel, Z. Ji, B. France, T. Xia, E. Suarez, R. Rallo, L. Madler, Y. Cohen, E. M. V. Hoek, A. Nel, *Nanoscale* **2011**, 3, 1345.

[3] T. F. Lin, J. K. Wu, *Water Res.* **2001**, 35, 2049.

- [4] B. Deng, M. Caviness, Z. Gu, *ACS Symp. Ser.* **2005**, 915, 284.
- [5] S. Yao, Z. Liu, Z. Shi, *J. Environ. Health. Sci. Eng.* **2014**, 12, 58.
- [6] Y. Jia, T. Luo, X.-Y. Yu, Z. Jin, B. Sun, J.-H. Liu, X.-J. Huang, *New J. Chem.* **2013**, 37, 2551.
- [7] H.-T. Fan, X. Fan, J. Li, M. Guo, D. Zhang, F. Yan, T. Sun, *Ind. Eng. Chem. Res.* **2012**, 51, 5216.
- [8] W. Driehaus, M. Jekel, U. Hildebrandt, *Aqua (Oxford)* **1998**, 47, 30.
- [9] T. S. Sreeprasad, S. M. Maliyekkal, K. P. Lisha, T. Pradeep, *J. Hazard. Mater.* **2011**, 186, 921.
- [10] W. Gao, M. Majumder, L. B. Alemany, T. N. Narayanan, M. A. Ibarra, B. K. Pradhan, P. M. Ajayan, *ACS Appl. Mater. Interfaces* **2011**, 3, 1821.
- [11] D. Koushik, S. Sen Gupta, S. M. Maliyekkal, T. Pradeep, *J. Hazard. Mater.* **2016**, 308, 192.
- [12] V. Chandra, J. Park, Y. Chun, J. W. Lee, I. C. Hwang, K. S. Kim, *ACS Nano* **2010**, 4, 3979.
- [13] U. Schwertmann, R. M. Cornell, *Iron Oxides in the Laboratory*, 2nd Ed., Wiley-VCH, Weinheim, Germany **2000**.
- [14] A. Navrotsky, L. Mazeina, J. Majzlan, *Science* **2008**, 319, 1635.
- [15] S. Dixit, J. G. Hering, *Environ. Sci. Technol.* **2003**, 37, 4182.
- [16] J. Gimenez, M. Martinez, J. de Pablo, M. Rovira, L. Duro, *J. Hazard. Mater.* **2007**, 141, 575.
- [17] Y. Jia, L. Xu, Z. Fang, G. P. Demopoulos, *Environ. Sci. Technol.* **2006**, 40, 3248.
- [18] A. Ghosh, Y. Krishnan, *Nat. Nanotechnol.* **2014**, 9, 491.
- [19] S. Das, M. J. Hendry, J. Essilfie-Dughan, *Environ. Sci. Technol.* **2011**, 45, 268.
- [20] M. U. Sankar, S. Aigal, S. M. Maliyekkal, A. Chaudhary, A. A. Anshup Kumar, K. Chaudhari, T. Pradeep, *Proc. Natl. Acad. Sci. USA* **2013**, 110, 8459.
- [21] V. K. Mourya, N. N. Inamdar, A. Tiwari, *Adv. Mater. Lett.* **2010**, 1, 11.
- [22] K. Rout, M. Mohapatra, S. Anand, *Dalton Trans.* **2012**, 41, 3302.
- [23] V. Gade, T. Dave, V. Chauhan, S. Dasaka, In *Proc. Indian Geotechnical Conf., Roorkee, Roorkee, India* **2013**.
- [24] D. Das, G. Samanta, B. K. Mandal, T. R. Chowdhury, C. R. Chanda, P. P. Chowdhury, G. K. Basu, D. Chakraborti, *Environ. Geochem. Health* **1996**, 18, 5.
- [25] S. Kumar, R. R. Nair, P. B. Pillai, S. N. Gupta, M. A. R. Iyengar, A. K. Sood, *ACS Appl. Mater. Interfaces* **2014**, 6, 17426.
- [26] A. P. Grosvenor, B. A. Kobe, M. C. Biesinger, N. S. McIntyre, *Surf. Interface Anal.* **2004**, 36, 1564.
- [27] R. P. Gupta, S. K. Sen, *Phys. Rev. B* **1974**, 10, 71.
- [28] K. M. Towe, W. J. Bradley, *J. Coll. Inter. Sci.* **1967**, 24, 384.
- [29] F. M. Michel, L. Ehm, S. M. Antao, P. L. Lee, P. J. Chupas, G. Liu, D. R. Strongin, M. A. Schoonen, B. L. Phillips, J. B. Parise, *Science* **2007**, 316, 1726.